Dalton Transactions

PAPER

View Article Online
View Journal | View Issue



Cite this: *Dalton Trans.*, 2018, **47**, 13368

# Platinum-based metallomesogens bearing a Pt(4,6-dfppy)(acac) skeleton: synthesis, photophysical properties and polarised phosphorescence application†

Xuefeng Yang,[c] Xiugang Wu,[a] Di Zhou,[c] Junting Yu,[e] Guohua Xie,*[b] Duncan W. Bruce *[d] and Yafei Wang *[a,b]

Polarised phosphorescence has a bright future in backlighting for conventional liquid crystal displays due to its theoretical 100% internal quantum efficiency and low cost. However, there are scarce reports on polarised phosphorescence from metallomesogens. In this contribution, a platinum-based metallomesogen containing a mesogenic biphenyl (**Pt1**) was prepared and characterised. To further explore the effect of the substituent on mesophase and emission properties, a related complex **Pt2** containing a tetraphenylethene (TPE) moiety was also synthesised. Both complexes melt at elevated temperatures but thereafter do not appear to crystallise on cooling. Complex **Pt1** shows an enantiotropic nematic phase from which a broad emission can be seen when spread as a film; in solution, an intense, sky-blue emission is observed. For **Pt2**, which shows a monotropic SmA phase, the emission in the condensed phase is suppressed and there is only weak emission in solution. Polarisation-dependent photoluminescence with a polarised ratio of 5.4 was obtained for the aligned film of a **Pt1**:polyimide mixture. Using **Pt1** as an emissive layer, non-doped, polarised organic light-emitting diodes presented a broad emission spectrum in the range of 450–900 nm with a polarised ratio of 1.33 and the highest external quantum efficiency of 1.1%. This research has an important significance for achieving broad-based polarised phosphorescence from platinum complex-based metallomesogens.

Received 24th July 2018,
Accepted 30th August 2018

DOI: 10.1039/c8dt03017k

rsc.li/dalton



## Introduction

Linearly polarised electroluminescent (EL) light is potentially useful as a backlight in traditional liquid crystal displays (LCDs) due to its low cost and reduced power consumption.[1–3] Over the past two decades, considerable work on polarised EL emission based on fluorescent liquid crystal materials (including polymers, oligomers and small molecules) has been reported.[4–8] Although relatively high dichroic ratios were realised for these fluorescence-based EL devices, the performance was limited by the intrinsic 25% internal quantum efficiency.

Phosphorescent metallomesogens, that is the metal-containing liquid crystals, are of interest to both chemists and physicists because of their unique mesomorphic properties based on the inclusion of the metal atom and the theoretical 100% internal quantum efficiency.[9–12] To date, a considerable number of phosphorescent metallomesogens have been designed and prepared[13–17] and the most effective strategy for the design of such materials has been the modification of known chromophores in such a way as to introduce the anisotropy necessary for liquid crystal phase formation. For example, phosphorescent metallomesogens based on lanthanides,[18–21] platinum,[22–34] iridium,[35–39] and palladium[40] have been reported. Among these, platinum-based metallomesogens were developed rapidly owing to their efficient emission and diverse emission states and the fact that the planar geometry of platinum(II) is well suited to the formation of

[a]*National Experimental Demonstration Center for Materials Science and Engineering (Changzhou University), Jiangsu Key Laboratory of Environmentally Friendly Polymeric Materials, Jiangsu Collaborative Innovation Center of Photovoltaic Science and Engineering, School of Materials Science & Engineering, Changzhou University, Changzhou 213164, China. E-mail: qiji830404@hotmail.com*
[b]*Hubei Key Lab on Organic and Polymeric Optoelectronic Materials, Department of Chemistry, Wuhan University, Wuhan 430072, China. E-mail: guohua.xie@whu.edu.cn*
[c]*College of Chemistry, Key Lab of Environment-Friendly Chemistry and Application of the Ministry of Education, Xiangtan University, Xiangtan 411105, China*
[d]*Department of Chemistry, University of York, Heslington, York, YO10 5DD, UK. E-mail: duncan.bruce@york.ac.uk*
[e]*Key Laboratory of Theoretical Organic Chemistry and Functional Molecule, Ministry of Education, College of Chemistry and Chemical Engineering, Hunan University of Science and Technology, Xiangtan 411201, P. R. China*

†Electronic supplementary information (ESI) available. CCDC 1827423. For ESI and crystallographic data in CIF or other electronic format see DOI: 10.1039/c8dt03017k

mesomorphic materials. Thus, several research groups have reported a series of platinum-based metallomesogens *via* the modification of phenylpyridine derivatives or by the use of functionalised ancillary ligands.[22–34] Intense phosphorescent emission with a fluorescence quantum yield ($\Phi_{lum}$) up to 0.5–0.7 was obtained for platinum-based metallomesogens at room temperature in solution.[41] Recently, cyclometalated iridium complexes were successfully used to realise phosphorescent metallomesogens, which possess high emission efficiency both in solution and in the condensed state.[35–39] Though with the use of the iridium complex with an octahedral geometry it is very difficult to realise the mesophase, it provides a novel method for achieving phosphorescent metallomesogens with high emission efficiency. Unfortunately, few reports on polarised phosphorescence, especially polarised electroluminescence, have been found from these luminescent metallomesogens.[33,42] Therefore, the question of how to balance emission efficiencies and dichroic ratios is a relatively new aspect of work with phosphorescent metallomesogens.

Therefore, the design of phosphorescent metallomesogens with efficient dichroic ratios and high emission efficiency is targeted *via* controlling the molecular structure. According to the previous work,[18] metallomesogens can be prepared through incorporating several flexible chains on the periphery, yet too many such chains often result in decreased emission efficiency due to the increased nonradiative transition. Herein, it is proposed that metallomesogens with a moderately rigid skeleton and fewer flexible chains could address the balance between dichroic ratio and emission efficiency. Hence, a platinum-based metallomesogen **Pt1** was synthesised, in which 2,4-difluorophenylpyridine was used as the cyclometalating ligand and an acetylacetone functionalised with mesogenic biphenyl units was employed as the ancillary ligand to induce liquid crystallinity. The fluorine atoms in the cyclometalating ligand and ancillary ligand can affect the emission wavelength *via* control of the LUMO energy and be effective in promoting mesomorphism, respectively. To further investigate the effect of substituents on the photophysical properties, another platinum complex (**Pt2**) bearing a tetraphenylethene (TPE) unit was prepared as TPE is known to induce aggregation-induced emission (AIE). The thermal and photophysical properties of both platinum complexes were investigated.

## Results and discussion

### Synthesis and structure

The synthetic route of both platinum complexes is illustrated in Scheme 1. A typical Suzuki coupling reaction between 2,5-dibromopyridine and (2,4-difluorophenyl)boronic acid catalyzed by $[Pd(PPh_3)_4]$ yielded the intermediate Brdfppy. 4,4,5,5-Tetramethyl-2-(4-(1,2,2-triphenylvinyl)phenyl)-1,3,2-dioxaborolane was then reacted with Brdffpy leading to the cyclometallating ligand TPE-dfppy in good yield. The key precursor of the acetylacetone derivative (ligand) was reported in previous work.[38] Finally, the target platinum complexes were prepared *via* a cyclometallation reaction between potassium tetrachloroplatinate(II) and the cyclometallating ligand (dfppy or TPE-dfppy) in 2-ethoxyethanol, followed by bridge cleavage with the functionalised acetylacetone derivative. Both platinum complexes were characterised by NMR spectroscopy, TOF-MS and elemental analysis.

### X-ray single crystal structure

Single crystals of complex **Pt1** were obtained by slow evaporation from a mixture of $CH_2Cl_2$/hexane at room temperature. The perspective view of **Pt1** is shown in Fig. 1 and Fig. S1,† and selected crystallographic data are listed in Table 1. The crystal structure of **Pt1** reveals that the skeleton of the platinum core possesses a square-planar geometry. The methylene spacers in the functionalised acac show an all-*trans* arrangement and this continues to the ether oxygen in only one of them. The Pt–Pt distance is 9.546 Å, which is too long to form effective solid-state metal–metal-to-ligand charge transfer, while the bond lengths of Pt–N (1.987(7) Å) and Pt–O (1.991(6) and 2.094(5) Å) are similar to those of common platinum complexes.

### Mesomorphic behaviour

Before exploring the mesomorphic properties of the platinum complexes, TGA measurement was carried out to evaluate their thermal stability. Notably, both complexes show good thermal stability with high decomposition temperatures (5% weight loss) over 325 °C (Table 2, Fig. S2†). Then the thermotropic behaviour of both platinum complexes was analysed by DSC (Fig. S3 and S4†) and polarised optical microscopy; the thermal data are summarised in Table 2.

On heating, complex **Pt1** melted at 118.3 °C to give a phase that was identified readily as nematic on the basis of its optical texture (Fig. 2). The phase persisted to 183.3 °C where it cleared to isotropic, reforming immediately on cooling. DSC evidence (Fig. S3†) shows that on cooling, the complex does not crystallise and reheating simply leads to the nematic clearing again at 183.3 °C. There is a small thermal event on reheating at 37.2 °C, but it does show a hysteresis of just over 7 °C suggesting that it is not a fluid mesophase. Its identity was not investigated further.

On heating **Pt2**, the complex was found to melt at 54 °C forming a SmA phase that persisted effectively until 110 °C at which point it cleared. Subsequent heat–cool cycles did not show a crystallisation event, although there is a suggestion of a possible glass transition close to the melting point. No good photomicrograph (Fig. S5†) is given for the SmA phase as the very fluid sample tended to agglomerate and was difficult to spread to create thin sections that persisted to allow digital optical capture. Nonetheless, on pressing the sample, a small fan texture along with the classical oily streak texture could be observed, making characterisation unequivocal. It is interesting to note that the same mesogenic unit – the modified acac – led to two different phases, nematic and SmA, in the two different compounds. Given the nature of **Pt1**, a nematic

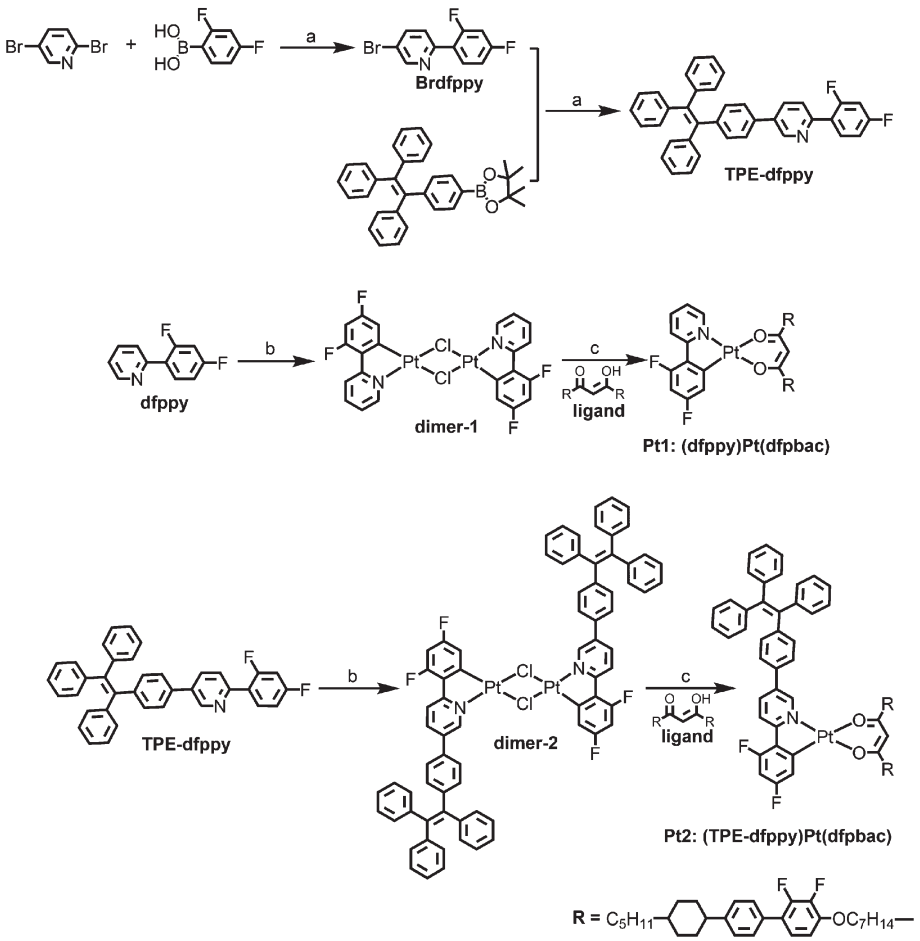


**Scheme 1** Synthetic route of platinum complexes. (a) $K_2CO_3$, $[Pd(PPh_3)_4]$, THF, reflux, overnight; (b) $K_2[PtCl_4]$, 2-ethoxyethanol, $H_2O$, 80 °C, 24 h; (c) acac derivative, $Na_2CO_3$, 2-ethoxyethanol, 100 °C, overnight.

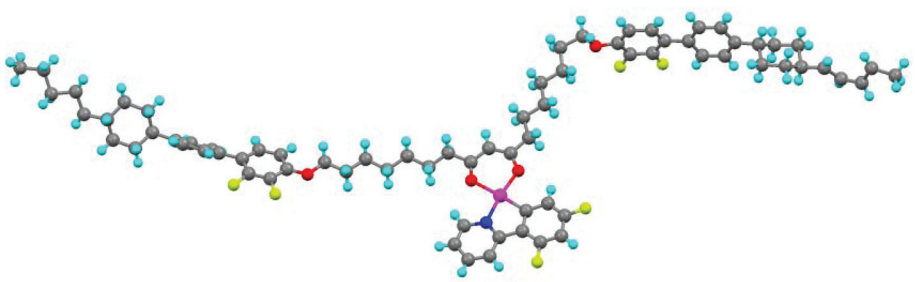

**Fig. 1** Molecular structure of complex **Pt1**.

phase is not surprising (difluoroterphenyl units), but that a SmA phase is seen in **Pt2** is likely related to the fact that the TPE moiety promotes AIE causing local self-assembly that supports the formation of a lamellar phase.

### Photophysical properties

The UV-vis absorption and photoluminescence (PL) spectra of both platinum complexes recorded in degassed $CH_2Cl_2$ solution ($10^{-5}$ M) are shown in Fig. 3, and the relevant data are listed in Table 3. Two clear absorption bands are observed for both platinum complexes. The absorption bands between 250 and 350 nm are assigned to the ligand-centered (LC) $^1\pi$–$\pi^*$ transitions while the absorption bands in the range of 350–450 nm are attributed to the mixture of LC $^3\pi$–$\pi^*$ and metal-to-ligand charge transfer (MLCT) transitions. The increased absorption intensity at 327 nm for complex **Pt2** originates from the additional TPE unit $^1\pi$–$\pi^*$ transition.[45,46] Compared to complex **Pt1**, complex **Pt2** possesses a red-shift

 

Table 1 Crystallographic data for **Pt1**

| | |
|---|---|
| Empirical formula | $C_{74}H_{83}F_6NO_4Pt$ |
| Formula weight | 1359.50 |
| Temperature/K | 173.0 |
| Crystal system | Triclinic |
| Space group | $P\bar{1}$ |
| $a$/Å | 9.4799(15) |
| $b$/Å | 11.2272(17) |
| $c$/Å | 32.541(5) |
| $\alpha$/° | 95.086(5) |
| $\beta$/° | 97.666(3) |
| $\gamma$/° | 108.351(3) |
| Volume/Å$^3$ | 3226.3(9) |
| $Z$ | 2 |
| $\rho_{calc.}$/g cm$^{-3}$ | 1.399 |
| $\mu$/mm$^{-1}$ | 2.242 |
| $F$(000) | 1396.0 |
| Crystal size/mm$^3$ | 0.19 × 0.15 × 0.11 |
| Radiation | MoKα ($\lambda$ = 0.71073) |
| 2Θ range for data collection/° | 2.55 to 52.856 |
| Index ranges | $-11 \le h \le 11$, $-12 \le k \le 13$, $-40 \le l \le 40$ |
| Reflections collected | 26 261 |
| Independent reflections | 12 931 [$R_{int}$ = 0.0846, $R_{sigma}$ = 0.1398] |
| Data/restraints/parameters | 12 931/783/777 |
| Goodness-of-fit on $F^2$ | 1.002 |
| Final $R$ indexes [$I >= 2\sigma(I)$] | $R_1$ = 0.0739, w$R_2$ = 0.1821 |
| Final $R$ indexes [all data] | $R_1$ = 0.1239, w$R_2$ = 0.2138 |
| Largest diff. peak/hole/e Å$^{-3}$ | 1.77/−1.43 |

Table 2 Phase-transition temperatures of platinum complexes

| Compound | Phase sequence[a] | $T$/°C[b] | $\Delta H$/kJ mol$^{-1}$ | $T_d$/°C |
|---|---|---|---|---|
| **Pt1** | Cr-N | 118.3 | 54.0 | 340 |
| | N-Iso | 183.3 | 3.1 | |
| **Pt2** | Cr-SmA | 54.0 | 34.6 | 325 |
| | SmA-Iso | 109.9 | 2.2 | |

[a] Cr = crystal, SmA = smectic A phase, N = nematic phase, and Iso = isotropic phase. [b] DSC data are onset temperatures.

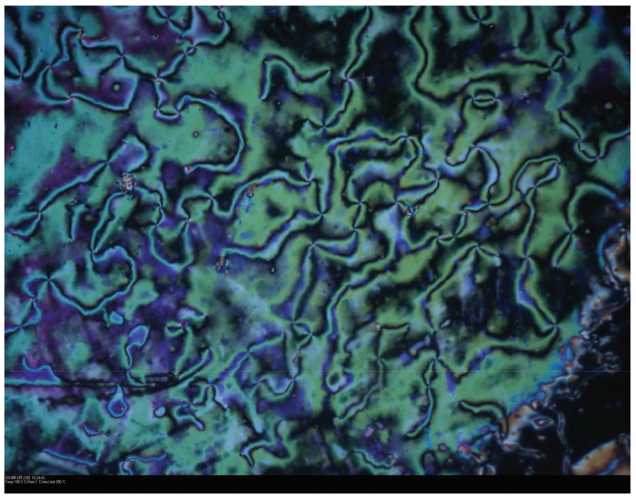

Fig. 2 Polarised optical micrograph of **Pt1** recorded on cooling from the isotropic state at 185 °C.

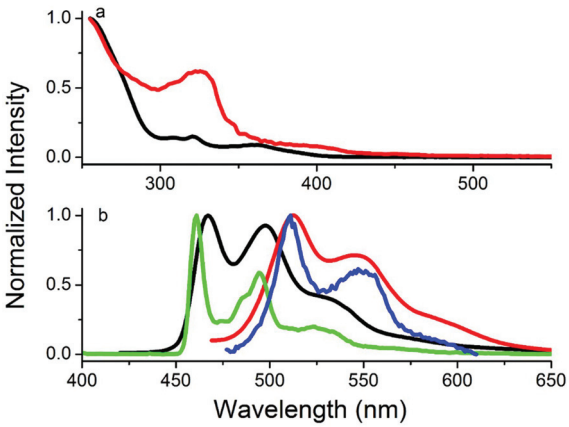


Fig. 3 UV-vis absorption (a) and emission spectra (b) of platinum complexes in degassed solution at room temperature (RT) and 77 K. Black line: **Pt1** at RT, red line: **Pt2** at RT, green line: **Pt1** at 77 K, and blue line: **Pt2** at 77 K.

absorption spectrum owing to its extended conjugation coursed by the conjugated TPE unit.

With an excitation wavelength of 395 nm, complex **Pt1** showed strong sky-blue emission with the maximum peak at 469 nm ($\Phi_{lum}$ = 28.2%), while complex **Pt2** presented a weak emission in the yellow-greenish region ($\Phi_{lum}$ = 3.8%) in degassed solution at room temperature. As shown in Fig. 3b, the structured PL profiles with the vibronic splitting at *ca.* 1380 cm$^{-1}$ in the emission bands, a typical aromatic stretching of the ligand, imply that the emission is mainly from a local excited (LC) state in both platinum complexes at room temperature. Meanwhile, the relatively long radiative decay lifetime (*ca.* 0.3 μs, Fig. S6†) of the complex **Pt1** suggests the involvement of the LC $^3(\pi$–$\pi^*)$ excited state in the emission. Due to the weak emission, the lifetime of complex **Pt2** was not detectable in solution at room temperature.

At 77 K in frozen toluene, both platinum complexes display well-dissolved vibronic structures with a hypsochromic shift compared to the PL profiles at room temperature (Fig. 3b), which is explained by the rigidochromic effect in low-temperature glasses. According to the previous report,[47] the magnitude of the thermally induced Stokes shift ($\Delta E_s$ = $E_{00}$(77 K) − $E_{00}$(300 K)) can be used to explain the nature of the lowest lying excited state in the platinum complex. Therefore, complexes **Pt1** and **Pt2** possess the $\Delta E_s$ of 279 and 114 cm$^{-1}$, respectively, implying LC emission. The decay lifetimes at 77 K (**Pt1**: 7.3 μs and **Pt2**: 13.4 μs, Fig. S7†) are clearly longer than those at room temperature (Table 1), caused by an increased nonradiative decay rate.

It is common for platinum complexes to form an excimer emission due to intermolecular Pt···Pt interactions and, to this end, the concentration-dependent luminescence was studied to investigate the possibility of intermolecular interaction. For complex **Pt1**, the intensity of the high-energy emission first increases after which it decreases sharply with the increasing concentration ($10^{-6}$–$10^{-2}$ M) due to aggregation-induced

Table 3 Photophysical data of both platinum complexes

| | $\lambda_{abs}$[a] (nm) ($10^5$ $M^{-1}$ $cm^{-1}$) | $\lambda_{em}$ (nm) | $\lambda_{em}$[d] (nm) | $\tau$ (μs) | $\Phi_{PL}$ (%)[g] | $\mu_h$ ($cm^2$ $V^{-1}$ $s^{-1}$) | $\mu_e$ |
|---|---|---|---|---|---|---|---|
| **Pt1** | 257 (1.46), 309 (0.20), 321 (0.22), 363 (0.13) | 467, 498, 535[b]<br>466, 500, 606[c] | 461, 495, 526 | 0.3[e]<br>7.3[f] | 28.2 | $1.74 \times 10^{-5}$ | $1.93 \times 10^{-4}$ |
| **Pt2** | 257 (0.16), 327 (0.11), 402 (0.01) | 512, 549, 593[b]<br>— | 511, 549 | —<br>13.4[f] | 3.8 | $1.91 \times 10^{-5}$ | $5.31 \times 10^{-4}$ |

a, b, e, and g: in $CH_2Cl_2$ solution, $10^{-5}$ M; c: in neat film; d and f: at 77 K in toluene.

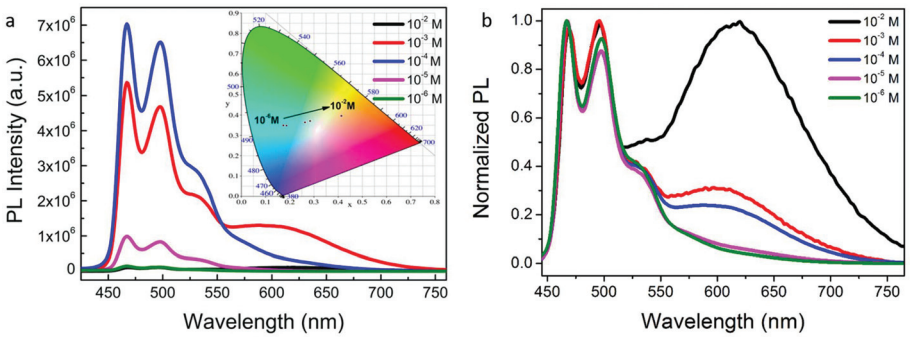


Fig. 4 Concentration-dependent emission spectra of **Pt1** in degassed $CH_2Cl_2$ (a: non-normalised; b: normalised), inset: the CIE coordinates for the concentration-dependent PL profiles.

quenching (Fig. 4a). Additionally, a long-wavelength emission at about 610 nm is observed whose emission intensity increases with increasing concentration (Fig. 4b), *i.e.* a typical excimer emission from the platinum complex. Correspondingly, the Commission Internationale de L'Eclairage (CIE) coordinates of the concentration-dependent PL profiles have a variation in the vicinity of the white emission region. In contrast, no excimer emission was found for complex **Pt2** in concentrated solution (Fig. S8†), most likely due to the steric size of TPE preventing the organisation necessary for intermolecular Pt⋯Pt interactions.

The emission in neat films displays a distinct difference from that in solution. Thus, an intense emission (Fig. S9†) peaking at 606 nm with the shoulders at 466 and 500 nm is observed for **Pt1** at room temperature, which suggests that Pt⋯Pt interactions are presented in the neat film. Additionally, the temperature-dependent PL emission demonstrates that there is a negligible change with temperature (Fig. S9†), implying that the different phases in the complex **Pt1** have little effect on the luminescence properties. As for complex **Pt2**, the cyclometallating ligand (TPE-dfppy) clearly leads to aggregation-induced emission properties, while its corresponding cyclometallated complex (**Pt2**, Fig. S10†) does not emit when in a neat film. This unusual photophysical phenomenon could be explained by the intramolecular charge transfer between the TPE unit (donor) and platinum skeleton (acceptor).

## Charge transfer mobilities

The hole and electron mobilities of both platinum complexes were measured using the space charge limited current (SCLC) method. The current density–voltage (*J*–*V*) curves are shown in Fig. 5, and the derived mobility values are listed in Table 3. The pristine films of the complexes **Pt1** and **Pt2** exhibit the hole mobilities of $1.74 \times 10^{-5}$ and $1.91 \times 10^{-5}$ $cm^2$ $V^{-1}$ $s^{-1}$, respectively, while their electron mobility values are in the region of $10^{-4}$ $cm^2$ $V^{-1}$ $s^{-1}$ (**Pt1**: $1.93 \times 10^{-4}$, **Pt2**: $5.31 \times 10^{-4}$). Compared with the hole mobilities, the complexes **Pt1** and **Pt2** have higher electron mobilities. Upon thermal annealing at 150 °C, only the hole mobility of the complex **Pt2** was detected to be $6.62 \times 10^{-4}$ $cm^2$ $V^{-1}$ $s^{-1}$, which has a clear enhancement compared to that of the pristine film.

## Polarised properties

The alignment film of complex **Pt1**:PI (polyimide) was prepared *via* the rubbing and annealing procedures as described in the Experimental section. The polarised images also prove that the annealed **Pt1**:PI mixture film is effectively aligned (Fig. 6b and c). Then the absorption and emission spectra of the aligned **Pt1**:PI mixture film were recorded with polarisation parallel (∥) and perpendicular to (⊥) the rubbing direction at room temperature. It is noted that there is a difference for both the absorption and emission profiles between pure complex **Pt1** and the aligned film, which could be explained by the molecular arrangement and the concentration of the platinum complex. The absorption intensity of the light polarised perpendicular ($A_\perp$) to the rubbing direction is clearly higher than that of the parallel orientation ($A_\parallel$) (Fig. S11†). As shown in Fig. 6a, the PL spectra exhibit distinct polarised-dependent broad emission in the range of 450–650 nm, implying that the polarised emission results from both the monomer and aggre-

 

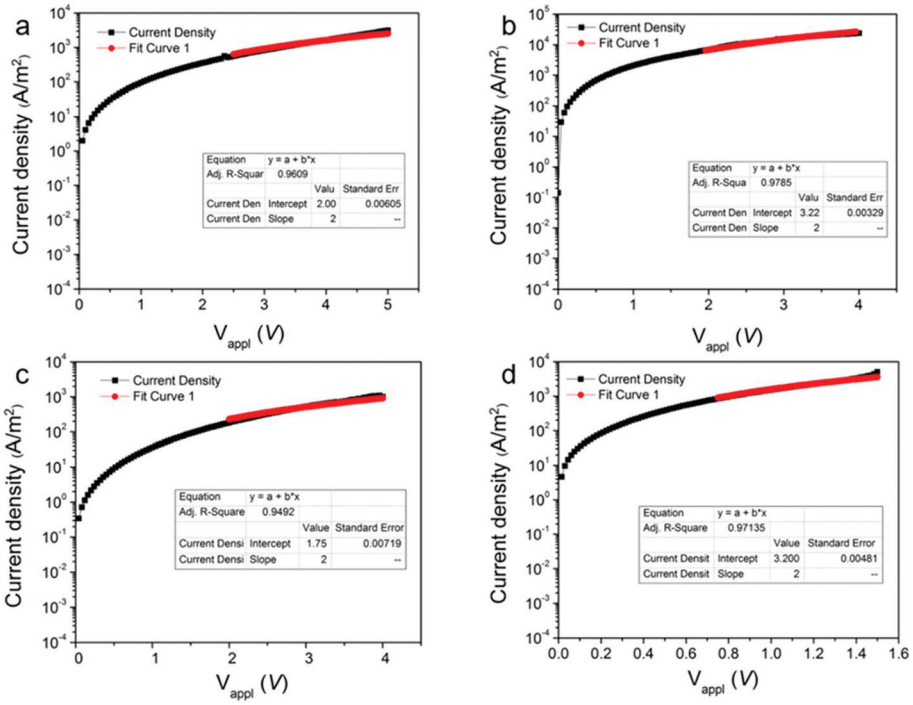


**Fig. 5** *J–V* plots for platinum complex-based hole-only/electron-only devices. (a) (**Pt1**) and (c) (**Pt2**) are hole-only devices; (b) (**Pt1**) and (d) (**Pt2**) are electron-only devices.

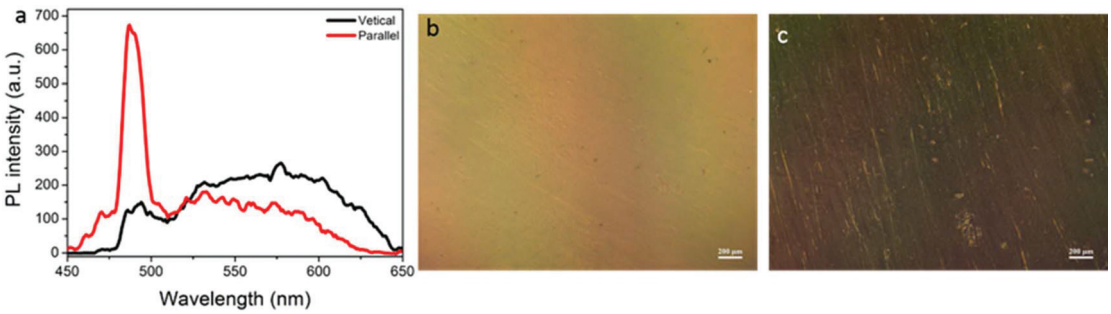


**Fig. 6** (a) PL spectra of the annealed **Pt1**:PI mixture film measured with the polarisation parallel and perpendicular to the rubbing direction. Alignment images under POM: (b) parallel with the rubbing direction; (c) perpendicular to the rubbing direction.

gation emissions (see above). At 485 nm, the emission intensity of the polarised film parallel to the rubbing direction is much stronger than that with the perpendicular orientation. The PL polarised ratio ($R$) is calculated from the relation of $R_{PL} = I_{\parallel}$ and $I_{\perp}$ to be 5.4, where $I_{\parallel}$ and $I_{\perp}$ are the maximum intensities of the film parallel and perpendicular to the rubbing direction, respectively. The optical order parameter ($S$) was estimated to be 0.56, using the equation of $S = \frac{I_{\parallel} - I_{\perp}}{I_{\parallel} + 2I_{\perp}}$.[48] This is indicative of a good alignment of the platinum complex upon the polyimide surface. However, the polarisation-dependent emission is reversed in the long-wavelength region (510–650 nm), *i.e.* $I_{\parallel}$ is weaker than $I_{\perp}$. This phenomenon implies that the monomolecular emission is roughly aligned with the rubbing direction while the aggrega-

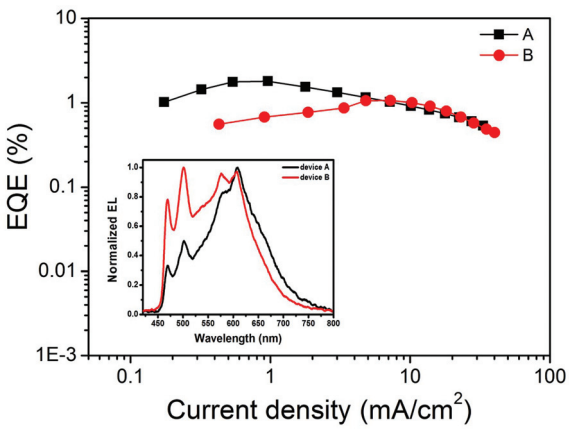


**Fig. 7** External quantum efficiency (EQE) curves of the devices A and B. Inset: EL spectra of the devices A and B at 10 V.

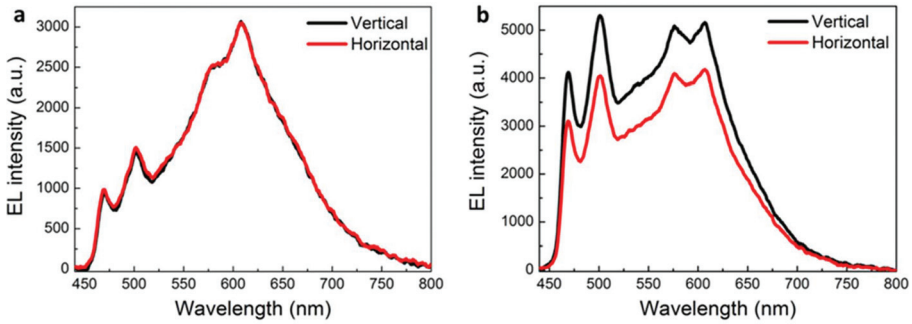


Fig. 8 Polarised EL spectra of the complex **Pt1** in the devices A (a) and B (b).

tion emission is perpendicular to the rubbing direction. The *R* and *S* values of the aggregation emission are also weaker than those of the monomer emission.[42]

### Polarised electroluminescence

To further investigate the polarised electroluminescence (EL) of the complex **Pt1**, non-doped devices with different procedures were fabricated with the same configuration of ITO/PEDOT:PSS (70 nm)/PVK (10 nm)/**Pt1** (30 nm)/TmPyPB (60 nm)/Liq (1 nm)/Al (100 nm). The detailed procedures are listed in the Experimental section.

As shown in Fig. 7, both devices showed analogous EL spectra in the range of 380–900 nm, which is similar to the PL spectra in the neat film. The emission bands between 450 nm and 500 nm are assigned to the intrinsic emission while the long wavelength emission is attributed to the excimer emission. The CIE coordinates of both devices A and B were calculated to be (0.47, 0.45) and (0.40, 0.45), respectively.

Clearly, very broad EL spectra with the polarised electroluminescence were observed in the device B rather than A, for which the EL polarised ratio of 1.33 (at 469 nm, Fig. 8) was calculated. This result demonstrated that a direct rubbing procedure for the emitter plays a key role in the polarised emission. The polarised profiles are similar to the PL emissions in the neat film, which means that the polarised emission is from the platinum complex. The tolerable device performances with the highest external quantum efficiencies (EQEs) of 1.8% and 1.1%, luminances of 227 and 230 cd $m^{-2}$ and current efficiencies of 2.8 and 1.7 cd $A^{-1}$ were achieved for the non-doped devices A and B, respectively (Fig. 7, 9 and S12†).

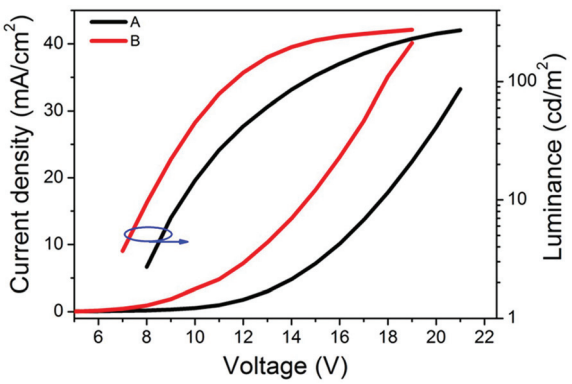


Fig. 9 Current density–voltage–luminance (*J*–*V*–*L*) curves of the complex **Pt1** in the devices A and B.

## Conclusions

In summary, two platinum complexes were prepared and characterised and X-ray single-crystal diffraction was performed for one of them. Complex **Pt1** displayed an enantiotropic nematic phase between 118 and 183 °C that appeared rather stable monotropically, only undergoing another transition at 38 °C on cooling. Complex **Pt2**, however, showed a monotropic SmA phase, which also persisted to ambient temperature without crystallisation. Intense emission was observed both in solution and in the neat film for the complex **Pt1** and polarisation-dependent absorption and emission spectra were achieved for the aligned **Pt1**:polyimide mixture film. Using **Pt1** as the emitter, the non-doped OLEDs presented broad polarised EL spectra in the range of 450–900 nm with a polarised ratio of 1.33, the maximum current efficiency of 1.7 cd $A^{-1}$ and the highest EQE of 1.1%. Unexpectedly, the introduction of the steric geometry TPE moiety into metallomesogens **Pt1** not only decreased the emission efficiency in solution and in the solid state but also destroyed the mesophase of complex **Pt2**. This research demonstrated that careful design of metallomesogens can enable metal complexes to have both high emission efficiency and efficient polarised emission and have a promising future in the field of polarised OLEDs.

## Experimental section

### Materials and measurements

2-(2,4-Difluorophenyl)pyridine was synthesised according to the reported procedure.[43] Other reagents were purchased from Energy Chemical Company Ltd and Aladdin companies. All reactions were carried out under a $N_2$ atmosphere. $^1$H NMR and $^{13}C\{^1H\}$ NMR spectra were acquired using a Bruker Dex-400 NMR instrument using $CDCl_3$ as a solvent. Mass spectra

 

(MS) were recorded on a Bruker Autoflex MALDI-TOF instrument using dithranol as a matrix. A molecular single crystal was measured by using a Bruker Smart Apex II. UV-vis absorption and photoluminescence (PL) spectra were recorded with a Varian Cray 50 and PerkinElmer LS50B luminescence spectrometer, respectively. Fluorescence lifetime measurements were recorded on an Edinburgh Instruments FLS-980 fluorescence spectrometer using time-correlated single photon counting (TCSPC). Absolute luminescent quantum yields were measured *via* a Quantaurus-QY. Polarised absorption and emission spectra were recorded by using a PerkinElmer Lambda 750 and PerkinElmer LS 55, respectively. Thermogravimetric analysis (TGA) was carried out with a NETZSCH STA449 from 25 °C to 600 °C at a heating rate of 20 °C $min^{-1}$ under a $N_2$ atmosphere. Differential scanning calorimetry (DSC) was carried out at the phase transition temperature with a rate of 20 °C $min^{-1}$ on the first heating cycle and 10 °C $min^{-1}$ in the first cooling and second heating processes. Polarised optical microscopy (POM) was carried out using an Olympus BX50 Optical Microscope equipped with a Linkam Scientific LTS350 heating stage, Linkam LNP2 cooling pump and Linkam TMS92 controller.

### Charge-carrier mobilities

Hole and electron mobilities were evaluated by the space charge limited current (SCLC) method with the configuration of ITO/PEDOT:PSS/platinum complex/$MoO_3$/Al for holes and ITO/ZnO/platinum complex/Ca/Al for electrons. The SCLC method is described by:

$$J = \frac{9\varepsilon_0\varepsilon_r\mu_0 V^2}{8L^3} \quad (1)$$

where $J$ (A $m^{-2}$) is the current density, $L$ is the film thickness of the platinum complex, $\mu_0$ ($cm^2$ $V^{-1}$ $s^{-1}$) is the hole or electron mobility, $\varepsilon_r$ (F $m^{-1}$) is the relative dielectric constant of the complex, $\varepsilon_0$ is the permittivity of free space ($8.85 \times 10^{-12}$ F $m^{-1}$), and $V$ ($V_{appl} - V_{bi}$) ($V$) is the internal voltage in the device, where $V_{appl}$ is the applied voltage to the device and $V_{bi}$ is the built-in voltage due to the relative work function difference of the two electrodes.[44]

### Alignment film

Polyimide (PI) solution was firstly added dropwise on a glass substrate. After being dried, the PI film was uniaxially rubbed several times with the dustless cloth. When the aligned PI film was heated to 190 °C, the platinum complex (**Pt1**) was added on the surface. The blend film was then annealed slowly after using another glass substrate with the same orientation covered on the prepared alignment film.

### Device fabrication and characterisation

A layer of poly(3,4-ethylenedioxythiophene):poly(styrenesulfonate) (PEDOT:PSS) was spin-coated on the ITO glass substrate after UV-ozone treatment. After baking PEDOT:PSS at 120 °C for 10 min, another layer of poly(*N*-vinylcarbazole) (PVK) was spin-coated directly and then baked at 120 °C for another 10 min. In order to obtain polarised emission, we treated the emitting layer *via* different methods (see below) after spin-coating of the complexes onto the hole transporting layer PVK. An electron transporting layer of 1,3,5-tri[(3-pyridyl)-phen-3-yl] benzene (TmPyPB) was thermally evaporated on the emitting layer. Liq and Al were used as the cathodes. All the devices were encapsulated under a nitrogen atmosphere using UV curable epoxy. The current–voltage–luminance characteristics were collected with a PR735 Spectrascan spectrometer and a Keithley 2400 programmable source meter. The (polarised) EL spectra were recorded by using an Ocean Optics USB2000 spectrometer. The EL intensities parallel and perpendicular to the rubbing direction (along the ITO stripe) could be distinguished by aligning a linear polariser inserted between the OLEDs and the spectrometer at two mutually perpendicular directions which were denoted as horizontal and vertical.

The device configurations are the same as the configuration of ITO/PEDOT:PSS (70 nm)/PVK (10 nm)/**Pt1** (30 nm)/TmPyPB (60 nm)/Liq (1 nm)/Al (100 nm). To further explore the effect of the alignment on the polarised emission, different alignment methods were tested for the active layer.

**Device A**: After spin-coating the complex **Pt1** onto PVK, the emissive layer was baked at 50 °C for 30 min.

**Device B**: In this method, the complex **Pt1** was directly rubbed with the dustless cloth after it was spin-coated onto PVK, and then baked at 50 °C for 30 min.

### Synthesis

**Synthesis of 5-bromo-2-(2,4-difluorophenyl)pyridine (Brdfppy).** A mixture of 2,5-dibromopyridine (7.50 g, 31.7 mmol), (2,4-difluorophenyl)boronic acid (5.0 g, 31.7 mmol), [$Pd(PPh_3)_4$] (730 mg, 0.63 mmol), aqueous $K_2CO_3$ (2 M, 15 mL) and THF (45 mL) was refluxed overnight under $N_2$. After cooling to RT, the reaction mixture was poured into 100 mL of water and extracted with $CH_2Cl_2$. The organic layers were washed with water and dried over $MgSO_4$ and the volatiles were removed under vacuum. The residue was purified by column chromatography on silica (petroleum ether/$CH_2Cl_2$ = 1 : 1) to obtain pure Brdfppy as a white solid (5.4 g, 64%). $^1$H NMR ($CDCl_3$, 400 MHz): $\delta$ (ppm): 8.78 (d, $J$ = 1.8 Hz, 1H), 8.06–8.00 (m, 1H), 7.92–7.89 (m, 1H), 7.71–7.69 (d, $J$ = 1.8 Hz, 1H), 7.29 (s, 1H), 7.06–7.01 (m, 1H), 6.97–6.92 (m, 1H).

**Synthesis of 2-(2,4-difluorophenyl)-5-(4-(1,2,2-triphenylvinyl) phenyl)pyridine (TPE-dfppy).** To a solution of 4,4,5,5-tetramethyl-2-(4-(1,2,2-triphenylvinyl)phenyl)-1,3,2-dioxaborolane (1.0 g, 2.2 mmol) and Brdfppy (590 mg, 2.2 mmol) in THF, a 2 M aqueous solution of $K_2CO_3$ (2 M, 15 mL) and [$Pd(PPh_3)_4$] (76 mg) was added. The mixture was refluxed overnight under $N_2$. After cooling to RT, the reaction mixture was poured into 100 mL of water and extracted with $CH_2Cl_2$. The organic layers were washed with water and dried over $MgSO_4$ and the volatiles were removed under vacuum. The residue was purified by column chromatography on silica (petroleum ether/$CH_2Cl_2$ = 2 : 1) to obtain pure TPE-dfppy as a white solid (940 mg, 82%). $^1$H NMR ($CDCl_3$, 400 MHz): $\delta$ (ppm): 8.90 (d, $J$ = 3 Hz, 1H),

8.08–8.02 (m, 1H), 7.80–7.78 (m, 1H), 7.40–7.38 (d, $J$ = 6 Hz, 2H), 7.16–6.99 (m, 19H), 6.95–6.90 (m, 1H).

**General procedures for cyclometalated platinum complexes.** A mixture of cyclometalating ligand (500 mg, 2.6 mmol) and $K_2[PtCl_4]$ (436 mg, 1.1 mmol) in a mixture of 2-ethoxyethanol (15 mL) and water (5 mL) was heated to 80 °C for 24 h. After cooling down to room temperature, the precipitate of the chloro-bridged platinum dimer was collected by filtration and washed with water and hexane. The yellow solid was used in the next step without any further purification. A mixture of dimer (1 eq.), ancillary ligand (2.2 eq.), $Na_2CO_3$ (10 eq.) and 2-ethoxyethanol was stirred at 100 °C overnight. After cooling down to room temperature, the volatiles are removed under vacuum and the residue was purified by silica gel chromatography (petroleum ether/$CH_2Cl_2$ = 1.5 : 1) to afford the target platinum complexes.

**Pt1**: yellow solid, yield: 58%. $^1$H NMR ($CDCl_3$, 400 MHz): $\delta$ (ppm): 9.01 (d, $J$ = 3 Hz, 1H), 7.97–7.95 (d, $J$ = 6 Hz, 1H), 7.82 (t, $J$ = 6 Hz, 1H), 7.43–7.41 (d, $J$ = 6 Hz, 4H), 7.28–7.26 (d, $J$ = 6 Hz, 6H), 7.17–7.04 (m, 4H), 6.78–6.74 (t, $J$ = 6 Hz, 2H), 6.60–6.54 (m, 1H), 5.50 (s, 1H), 4.07–4.03 (m, 4H), 2.53–2.47 (t, $J$ = 18 Hz, 2H), 2.31–2.27 (t, $J$ = 12 Hz, 4H), 1.94–1.75 (m, 16H), 1.53–1.42 (m, 15H), 1.35–1.20 (m, 18H), 1.11–1.05 (m, 4H). $^{13}$C{$^1$H} NMR (100 MHz, $CDCl_3$, TMS), $\delta$ (ppm): 189.17, 187.66, 147.67, 147.57, 147.45, 147.37, 147.13, 138.71, 132.43, 132.34, 128.60, 127.03, 123.51, 123.47, 121.51, 123.47, 121.16, 121.15, 109.53, 101.96, 99.29, 69.82, 44.37, 41.12, 37.40, 37.34, 34.32, 33.61, 33.24, 29.21, 29.17, 29.12, 29.07, 26.67, 26.41, 26.29, 25.84, 25.67, 22.74, 14.13. $^{19}$F NMR (282 MHz, $CDCl_3$) $\delta$ (ppm): −106.698 (d, $J$ = 9.3 Hz), −112.15 (d, $J$ = 9.6 Hz), −141.98 (q, $J$ = 20.0 Hz), −158.98 (q, $J$ = 17.2 Hz). TOF-MS: 1365. EA (%): Calculated for $C_{74}H_{89}F_6NO_4Pt$: C 65.09, H 6.57, N 1.03; found: C 65.33, H 6.61, N 1.01.

**Pt2**: yellow solid, yield: 52%. $^1$H NMR ($CDCl_3$, 400 MHz): $\delta$ (ppm): 9.28 (s, 1H), 7.99–7.92 (m, 2H), 7.43–7.36 (m, 6H).7.28–7.26 (d, $J$ = 6 Hz, 5H), 7.17–7.01 (m, 20H), 6.77–6.69 (m, 2H), 6.59–6.54 (m, 1H), 5.48 (s, 1H), 4.06–3.97 (m, 4H), 2.50 (t, $J$ = 9 Hz, 2H), 2.30–2.26 (m, 3H), 2.02 (s, 2H), 1.94–1.75 (m, 13H), 1.52–1.26 (m, 35H), 1.11–1.02 (m, 4H). $^{13}$C{$^1$H} NMR (100 MHz, $CDCl_3$, TMS), $\delta$ (ppm): 188.87, 187.59, 147.67, 147.56, 147.43, 145.11, 144.53, 143.46, 143.39, 141.97, 139.91, 136.19, 133.75, 133.55, 132.43, 131.38, 131.33, 131.28, 128.60, 127.87, 127.82, 127.70, 127.04, 126.73, 126.70, 126.64, 125.73, 125.66, 123.51, 123.47, 122.99, 109.52, 102.00, 99.33, 69.78, 44.37, 40.79, 40.22, 37.41, 37.34, 34.32, 33.61, 32.24, 29.72, 29.29, 29.12, 29.07, 26.68, 26.40, 25.93, 25.81, 25.67, 22.74, 14.14. $^{19}$F NMR (282 MHz, $CDCl_3$) $\delta$ (ppm): −106.72 (d, $J$ = 9.9 Hz), −112.37 (d, $J$ = 9.3 Hz), −141.95 (q, $J$ = 28.5 Hz), −158.87 (q, $J$ = 19.7 Hz). TOF-MS: 1696. EA (%): Calculated for $C_{100}H_{107}F_6NO_4Pt$: C 70.82, H 6.36, N 0.83; found: C 70.36, H 6.57, N 1.01.

## Conflicts of interest

There are no conflicts to declare.

## Acknowledgements

Financial support is acknowledged from the National Natural Science Foundation of China (51773021, U1663229, 51473140), the Natural Science Foundation of Hunan Province (2017JJ2245) and the Talent project of Jiangsu Specially-Appointed Professor. We really thank Bowen Yang and Prof. Haifeng Yu (Department of Materials Science and Engineering, Peking University) for their support at polarised absorption and emission.

## References

1 M. Jandke, P. Strohriegl, J. Gmeiner, W. Brütting and M. Schwoerer, *Adv. Mater.*, 1999, **11**, 1518–1521.
2 P. Dyreklev, M. Berggren, O. Inganäs, M. R. Andersson, O. Wennerström and T. Hjertberg, *Adv. Mater.*, 1995, **7**, 43–45.
3 Y. F. Wang, J. W. Shi, J. H. Chen, W. G. Zhu and B. Etienne, *J. Mater. Chem. C*, 2015, **3**, 7993–8005.
4 M. Misaki, M. Chikamatsu, Y. Yoshida, R. Azumi, N. Tanigaki, K. Yase, S. Nagamatsu and Y. Ueda, *Appl. Phys. Lett.*, 2008, **93**, 023304–023306.
5 M. Jandke, P. Strohriegl, J. Gmeiner, W. Brütting and M. Schwoerer, *Synth. Met.*, 2000, **111–112**, 177–180.
6 S. W. Culligan, Y. Geng, S. H. Chen, K. Klubek, K. M. Vaeth and C. W. Tang, *Adv. Mater.*, 2003, **15**, 1176–1180.
7 A. C. A. Chen, S. W. Culligan, Y. Geng, S. H. Chen, K. Klubek, K. Vaeth and C. W. Tang, *Adv. Mater.*, 2004, **16**, 783–788.
8 H. Tokuhisa, M. Era and T. Tsutsui, *Appl. Phys. Lett.*, 1998, **72**, 2639–2641.
9 J. L. Serrano, *Metallomesogens, Synthesis, Properties and Applications*, VCH, Weinheim, New York, Basel, Cambridge, Tokyo, 1996, ISBN 3-527-29296-9.
10 D. W. Bruce, D. O'Hare and R. I. Walton, *Molecular Materials, Chapter 2, Physical Properties of Metallomesogens*, John Wiley & Sons, Ltd., 2010, ISBN 978-0-470-98677-6.
11 S. Guerra, T. Dutronc, E. Terazzi, K. Buchwalder, L. Guenee, R. Deschenaux, S. V. Eliseeva, S. Petoud and C. Piguet, *Coord. Chem. Rev.*, 2017, **340**, 79–97.
12 D. Kim, D. Kang, M. Lee, K. Jeong, J. Kim and C. Lee, *Chem. Commun.*, 2016, **52**, 12821–12824.
13 N. S. S. Kumar, M. Z. Shafikov, A. C. Whitwood, B. Donnio, P. B. Karadakov, V. N. Kozhevnikov and D. W. Bruce, *Chem. – Eur. J.*, 2016, **22**, 8215–8233.
14 N. M. M. Moura, C. Cuerva, J. A. S. Cavaleiro, R. F. Mendes, F. A. A. Paz, M. Cano, M. G. P. M. S. Neves and C. Lodeiro, *ChemPlusChem*, 2016, **81**, 262–273.
15 C. Cuerva, J. A. Campo, M. Cano and C. Lodeiro, *Chem. – Eur. J.*, 2016, **22**, 10168–10178.
16 R. Chico, C. Domínguez, B. Donnio, B. Heinrich, S. Coco and P. Espinet, *Cryst. Growth Des.*, 2016, **16**, 6984–6991.
17 I. S. Shashikala and D. W. Bruce, *Dalton Trans.*, 2008, 1128–1131.

 

18 K. Binnemans, *J. Mater. Chem.*, 2009, **19**, 448–453.
19 S. Suárez, D. Imbert, F. Gumy, C. Piguet and J. C. G. Bünzli, *Chem. Mater.*, 2004, **16**, 3257–3266.
20 Y. Galyametdinov, A. A. Knyazev, V. I. Dzhabarov, T. Cardinaels, K. Driesen, C. Görller-Walrand and K. Binnemans, *Adv. Mater.*, 2008, **20**, 252–257.
21 A. A. Knyazev, E. Y. Molostova, A. S. Krupin, B. Heinrich, B. Donnio, W. Haase and Y. Galyametdinov, *Liq. Cryst.*, 2013, **40**, 857–863.
22 S. L. Zhang, K. J. Luo, H. Geng, H. L. Ni, H. F. Wang and Q. Li, *Dalton Trans.*, 2017, **46**, 899–906.
23 C. Damm, G. Israel, T. Heqmann and C. Tschierske, *J. Mater. Chem.*, 2006, **16**, 1808–1816.
24 H. Geng, K. J. Luo, G. Zuo, L. Zhao, H. F. Wang, Q. Li and H. L. Ni, *Dyes Pigm.*, 2018, **149**, 82–91.
25 X. Y. Li, J. N. Hu, Y. Wu, R. Li, D. D. Xiao, W. Zeng, D. Q. Zhang, Y. J. Xiang and W. S. Jin, *Dyes Pigm.*, 2017, **141**, 188–194.
26 A. Santoro, A. C. Whitwood, J. A. G. Williams, V. N. Kozhevnikov and D. W. Bruce, *Chem. Mater.*, 2009, **21**, 3871–3882.
27 V. Kozhevnikov, B. Donnio and D. W. Bruce, *Angew. Chem., Int. Ed.*, 2008, **47**, 6286–6289.
28 C. Liao, H. Chen, H. Hsu, A. Poloek, H. Yeh, Y. Chi, K. Wang, C. Lai, G. Lee, C. Shih and P. Chou, *Chem. – Eur. J.*, 2011, **17**, 546–556.
29 M. Krikorian, S. Liu and T. M. Swager, *J. Am. Chem. Soc.*, 2014, **136**, 2952–2955.
30 A. Santoro, M. Wegrzyn, A. C. Whitwood, B. Donnio and D. W. Bruce, *J. Am. Chem. Soc.*, 2010, **132**, 10689–10691.
31 Y. Wang, Y. Liu, J. Luo, H. Qi, X. Li, M. Ni, M. Liu, D. Shi, W. Zhu and Y. Cao, *Dalton Trans.*, 2011, **40**, 5046–5051.
32 Y. Wang, Q. Chen, Y. Li, Y. Liu, H. Tan, J. Yu, M. Zhu, H. Wu, W. Zhu and Y. Cao, *J. Phys. Chem. C*, 2012, **116**, 5908–5914.
33 Y. F. Wang, J. Fan, J. W. Shi, H. R. Qi, E. Baranoff, G. H. Xie, Q. G. Li, H. Tan, Y. Liu and W. G. Zhu, *Dyes Pigm.*, 2016, **133**, 238–247.
34 J. W. Shi, Y. F. Wang, M. J. Xiao, P. Zhong, Y. Liu, H. Tan, M. X. Zhu and W. G. Zhu, *Tetrahedron*, 2015, **71**, 463–469.
35 E. I. Szerb, A. M. Talarico, I. Aiello, A. Crispini, N. Godbert, D. Pucci, T. Pugliese and M. Ghedini, *Eur. J. Inorg. Chem.*, 2010, **21**, 3270–3277.
36 A. M. Talarica, M. Ghedini, C. O. Rossi and E. L. Szerb, *Soft Matter*, 2012, **8**, 11661–11669.
37 A. Santoro, A. Prokhorov, V. N. Kozhevnikov, A. C. Whitwood, B. Donnio, J. A. G. Williams and D. W. Bruce, *J. Am. Chem. Soc.*, 2011, **133**, 5248–5251.
38 Y. F. Wang, C. P. Cabry, M. J. Xiao, D. W. Bruce, J. W. Shi, W. G. Zhu and E. Baranoff, *Chem. – Eur. J.*, 2016, **22**, 1618–1621.
39 X. Wu, G. Xie, C. P. Cabry, X. Xu, S. Cowling, D. W. Bruce, W. Zhu, E. D. Baranoff and Y. F. Wang, *J. Mater. Chem. C*, 2018, **6**, 3298–3309.
40 E. Tritto, R. Chico, G. Sanz-Enguita, C. L. Folcia, J. Ortega, S. Coco and P. Espinet, *Inorg. Chem.*, 2014, **53**, 3449–3455.
41 M. Spencer, A. Santoro, G. Freeman, A. Diez, P. R. Murry, J. Torroba, A. C. Whitwood, L. J. Yellowlees, J. A. G. Williams and D. W. Bruce, *Dalton Trans.*, 2012, **41**, 14244–14256.
42 S. Liu and M. Lin, *Org. Electron.*, 2011, **12**, 15–21.
43 Y. You and S. Y. Park, *J. Am. Chem. Soc.*, 2005, **127**, 12438–12439.
44 B. Kan and Q. Zhang, *J. Am. Chem. Soc.*, 2014, **136**, 15529–15532.
45 W. Z. Yuan, Z. Q. Yu, P. Lu, C. Deng, J. W. Y. Lam, Z. Wang, E.-Q. Chen, Y.-G. Ma and B. Z. Tang, *J. Mater. Chem.*, 2012, **22**, 3323–3326.
46 Y. F. Wang, Y. W. Liao, C. Cabry, D. Zhou, G. Xie, Z. Qu, D. Bruce and W. Zhu, *J. Mater. Chem. C*, 2017, **5**, 3999–4008.
47 A. Chakraborty, J. C. Deaton, A. Haefele and F. N. Castellano, *Organometallics*, 2013, **32**, 3819–3829.
48 T. Sato, H. Awano, O. Haba, H. Katagiri, Y.-J. Pu, T. Takahashi and K. Yonetake, *Dalton Trans.*, 2012, **41**, 8379–8389.